Fig. 8. Result yielded by the adaptive α-trimmed filter.

Fig. 9. Result yielded by the quadratic Type 1B filter.

a specific action of *THEN- ELSE* type, which is very well-suited to signal and image processing applications. Moreover, this mechanism allows *THEN*-rules to be conveniently grouped into subrulebases and effectively integrated [10].

REFERENCES

[1] S. K. Pal and A. Rosenfeld, "Image enhancement and tresholding by optimization of fuzzy compactness," *Patt. Recogn. Lett.*, vol. 7, no. 2, pp. 77–86, Feb. 1988.

[2] H. Li and H. S. Yang, "Fast and reliable image enhancement using fuzzy relaxation technique," *IEEE Trans. Syst., Man, Cybern.*, vol. SMC-19, no. 5, pp 1276–1281, Sept./Oct. 1989.

[3] D. Bhandari, S. K. Pal, and M. K. Kundu, "Image enhancement incorporating fuzzy fitness function in genetic algorithms," in *Proc. Second IEEE Int. Conf. Fuzzy Syst.*, San Francisco, Mar. 28–Apr. 1, 1993, pp. 1408–1413.

[4] S. K. Pal and R. A. King, "Image enhancement using smoothing with fuzzy sets," *IEEE Trans. Syst., Man, Cybern.*, vol. SMC-11, no. 7, pp. 494–501, July 1981.

[5] O. K. AlShaykh, S. Ramaswamy, and H.-S. Hung, "Fuzzy techniques for image enhancement and reconstruction," in *Proc. Second IEEE Int. Conf. Fuzzy Syst.*, San Francisco, Mar. 28-Apr. 1, 1993, pp. 582–587.

[6] F. Russo, "A user-friendly research tool for image processing with fuzzy rules," in *Proc. First IEEE Int. Conf. Fuzzy Syst.*, San Diego, Mar. 8–12, 1992, pp. 561–568.

[7] F. Russo and G. Ramponi, "Working on image data using fuzzy rules," in *Proc. Sixth Euro. Signal Processing Conf.*, Brussels, Belgium, Aug. 24-27, 1992, pp. 1413-1416.

[8] F. Russo and G. Ramponi, "Fuzzy operator for sharpening of noisy images," *IEE Electron. Lett.*, vol. 28, no. 18, Aug. 27, 1992, pp. 1715–1717.

[9] ——, "Nonlinear fuzzy operators for image processing," *Signal Processing*, vol. 38, no. 3, pp. 429–440 Aug. 1994.

[10] F. Russo, "A new class of fuzzy operators for image processing: design and implementation," in *Proc. Second IEEE Int. Conf. Fuzzy Systems*, San Francisco, CA, Mar. 28–Apr. 1, 1993, pp. 815-820.

[11] S. K. Mitra, H. Li, I.-S. Lin, and T-H. Yu, "A new class of nonlinear filters for image enhancement," in *Proc. IEEE Int. Conf. Acoust., Speech Signal Processing ICASSP-91*, Toronto, May 1991, pp. 2525–2528.

[12] A. Restrepo and A.C. Bovik, "Adaptive trimmed mean filters for image restoration," *IEEE Trans. Acoust., Speech Signal Processing*, vol. 36, no. 8, pp. 1326-1337, Aug. 1988.

Image Restoration Using the W-Slice Method

Elisa Sayrol, Chrysostomos L. Nikias, and Antoni Gasull

***Abstract*—We propose the use of higher order statistics (HOS)-based methods to address the problem of image restoration. The restoration strategy is based on the fact that the phase information of the original image and its HOS are not distorted by some types of blurring. The difficulties associated with the combination of 2-D signals and their HOS are reduced by means of the Radon transform. Two methods that apply the weight-slice algorithm over the projections are developed. Simulation results illustrate the performance of the proposed methods.**

I. INTRODUCTION

Higher order statistics (HOS) have been successfully applied to the problem of 2-D signal reconstruction. In [1], the phase of the Bispectrum is used to reconstruct images degraded by a jittery channel with additive tone interference, whereas in [2], the bispectrum is used to estimate a randomly translating and rotating object from a sequence of noisy images. Another application of HOS in a 2-D context is described in [3], where invariant HOS features of projections are used for object classification. One of the first applications of HOS

Manuscript received June 19, 1993; revised September 28, 1994. This work was supported by the Office of Naval Research under contract N00014-92-J-1034 and the Spanish Ministry of Education and Science. Portions of this paper were presented at the IEEE Signal Processing Workshop on Higher Order Statistics, South Lake Tahoe, CA, June 1993.

E. Sayrol and A. Gasull are with the Universitat Politècnica de Catalunya, E.T.S.E. Telecomunicació, Barcelona, Spain.

C. L. Nikias is with the Center for Research in Applied Signal Processing, University of Southern California, Los Angeles, CA 90089-2564 USA.

IEEE Log Number 9412460.

to image processing was to employ triple correlations to reconstruct astronomical images from short-exposure photographs [4], [5].

The bispectrum $B_f(w_1, w_2)$ of a 1-D, deterministic, discrete-time signal $f(n)$ is defined as the Fourier transform (FT) of its triple correlation function and is given by [6, ch. 3]

$$B_f(w_1, w_2) = F(w_1)F(w_2)F^*(w_1 + w_2) \tag{1}$$

where $F(w)$ is the FT of $f(n)$. The phase of the bispectrum is therefore

$$\psi_f(w_1, w_2) = \varphi_f(w_1) + \varphi_f(w_2) - \varphi_f(w_1 + w_2), \tag{2}$$

where $\psi_f(w_1, w_2) = \angle B_f(w_1, w_2)$ and $\varphi_f(w) = \angle F(w)$. Unlike the power spectrum, the bispectrum preserves the Fourier phase of the signal up to a linear phase factor. For a random signal, it can be defined as the statistical expectation of (1). The bispectrum of a zero-mean random process with symmetric probability density function (pdf) equals zero. Hence, deterministic signals embedded in Gaussian or non-Gaussian symmetrically distributed noise can be reconstructed in the third-order domain. Our goal is to exploit such properties for the restoration of 2-D degraded images.

We have developed techniques that consider HOS-based methods that proved to attain good 1-D signal reconstruction. In [7], the bispectrum iterative reconstruction algorithm (BIRA) [8] was utilized to restore images from their projections. However, the BIRA algorithm could not be applied to those projections that had Z-transform with zeros on the unit circle. The weight-slice (WS) algorithm [9], on the other hand, can recover the signal of interest even if its Z-transform has zeros on the unit circle. Although possible, the extension of the WS algorithm to 2-D would enormously increase its analytical complexity. We present two algorithms that use the WS method over the 1-D projections of the image.

In Section II, we describe the assumptions of the image observation model. In Section III, we set the bases for the reconstruction from either the phase of the Fourier transform or the phase of the bispectrum. In Section IV, two image restoration algorithms are developed. Some examples are given in Section V. Finally, Section VI is devoted to conclusions.

II. Preliminary Definitions

To address the problem of recovering images from degraded versions of it, we assume the discrete image model given by

$$\begin{aligned} g(n, m) &= \sum_{n'} \sum_{m'} h(n - n', m - m') f(n', m') \\ &\quad + n_o(n, m) \\ &= a(n, m) + n_o(n, m), \quad n'm' \in S, \end{aligned} \tag{3}$$

where

$g(n, m)$	observed image
$h(n, m)$	point spread function that can be deterministic or random
S	region of support of $h(m, n)$
$f(n, m)$	original undistorted image
$n_o(n, m)$	symmetrically distributed noise
$a(n, m)$	2-D convolution of $h(n, m)$ and $f(n, m)$.

The 2-D signal recovery problem can be uniquely decomposed into many 1-D signal reconstruction problems. The Radon transform of a 2-D function $f(n, m)$ denoted $f_\theta(s)$ is defined as its line integral along a line inclined at an angle θ from the y axis and at a distance s from the origin [10]. Denoting by $G_\theta(\xi)$, $A_\theta(\xi)$, $H_\theta(\xi)$ and $F_\theta(\xi)$ the Fourier transforms in polar coordinates of $g(n, m)$, $a(n, m)$, $h(n, m)$, and $f(n, m)$, respectively, then, in the absence of noise

$$G_\theta(\xi) = A_\theta(\xi) = H_\theta(\xi)F_\theta(\xi), \tag{4}$$

or taking the inverse Fourier transform

$$g_\theta(s) = a_\theta(s) = h_\theta(s) * f_\theta(s). \tag{5}$$

We can derive similar expressions for the projections of the bispectrum. Denoting by $B_{g\theta}(\xi_1, \xi_2)$, $B_{a\theta}(\xi_1, \xi_2)$, $B_{h\theta}(\xi_1, \xi_2)$, and $B_{f\theta}(\xi_1, \xi_2)$ the bispectra of $g_\theta(s)$, $a_\theta(s)$, $h_\theta(s)$, and $f_\theta(s)$, respectively, we obtain

$$\begin{aligned} B_{g\theta}(\xi_1, \xi_2) &= B_{a\theta}(\xi_1, \xi_2) \\ &= G_\theta(\xi_1)G_\theta(\xi_2)G_\theta^*(\xi_1 + \xi_2) \\ &= H_\theta(\xi_1)F_\theta(\xi_1)H_\theta(\xi_2)F_\theta(\xi_2) \\ &\quad H_\theta^*(\xi_1 + \xi_2)F_\theta^*(\xi_1 + \xi_2) \\ &= B_{h\theta}(\xi_1, \xi_2)B_{f\theta}(\xi_1, \xi_2). \end{aligned} \tag{6}$$

Our purpose is to recover each projection $f_\theta(s)$ in nonideal conditions. Next, we shall study two possible situations in which the reconstruction is possible: first, when the image is degraded by a deterministic PSF and additive noise and second, when the PSF is random.

A. Deterministic Blur Model

We consider the optical transfer function (OTF), which is the Fourier transform of the PSF, to have linear or zero phase [11]. Let $\varphi_{g\theta}(\xi)$, $\varphi_{a\theta}(\xi)$, and $\varphi_{f\theta}(\xi)$ be the phase functions of $G_\theta(\xi)$, $A_\theta(\xi)$, $F_\theta(\xi)$, respectively. Let us also denote by $\psi_{g\theta}(\xi_1, \xi_2)$, $\psi_{a\theta}(\xi_1, \xi_2)$, and $\psi_{f\theta}(\xi_1, \xi_2)$ the phase functions of $B_{g\theta}(\xi_1, \xi_2)$, $B_{a\theta}(\xi_1, \xi_2)$, and $B_{f\theta}(\xi_1, \xi_2)$. As it can be seen in (4), if the phase of the OTF is linear, the phase of the 1-D Fourier transform of a projection differs from the phase of the Fourier transform of the projection of the original image by a linear factor, and therefore, $\varphi_{g\theta}(\xi) = \varphi_{a\theta}(\xi) = \tau_{o\xi} + \varphi_{f\theta}(\xi)$, where τ_o characterizes the phase of the OTF. If τ_o is zero, they are equivalent $\varphi_{g\theta}(\xi) = \varphi_{f\theta}(\xi)$. In the third-order domain, $\psi_{g\theta}(\xi_1, \xi_2) = \psi_{a\theta}(\xi_1, \xi_2) = \psi_{f\theta}(\xi_1, \xi_2)$, where the linear phase component has been canceled out. $F_\theta(\xi)$ and $B_{f\theta}(\xi_1, \xi_2)$ are uniquely specified, except for a constant factor, by $\varphi_{f\theta}(\xi)$ and $\psi_{f\theta}(\xi_1, \xi_2)$, respectively, as is explained in Section III.

When the signal of interest is contaminated with noise, reconstruction from the phase functions is no longer acceptable. Nevertheless, we can estimate the bispectra of the projections in the case many independent, although possibly shifted, observations of the image are available. We will study the statistical properties of the estimation and take advantage, as stated above, of the fact that third-order statistics of zero-mean symmetrically distributed noise are zero. Our immediate goal is to obtain a good estimation of $B_{a\theta}(\xi_1, \xi_2)$ and, therefore, $\psi_{f\theta}(\xi_1, \xi_2)$ or $\varphi_{g\theta}(\xi)$. It can be shown that when the relative shift among the projections has a uniform or triangular distribution, the bispectrum estimation is only biased near the origin and limited to the axis $\xi_1 = 0$, $\xi_2 = 0$, and $\xi_1 + \xi_2 = 0$ for white noise. We can also take advantage of the fact that the phase of the bispectrum is zero at the origin, where the magnitude is biased and then approximate $\psi_{f\theta}(\xi_1, \xi_2)$ by $\psi_{a\theta}(\xi_1, \xi_2)$, from which we can reconstruct the signal of interest.

B. Random Blur Model

In astronomical speckle interferometry, speckle masking is a method based on triple correlations that is capable of reconstructing true diffraction-limited images [4]. Without loss of generality and since we process the projections of the image, the description is given in 1-D. A sequence of short exposure speckle interferograms $i_n(x)$ is given by

$$i_n(x) = o_n(x) * p_n(x) \tag{7}$$

where $o_n(x)$ is the intensity distribution of the object, and $p_n(x)$ is a random PSF combination of the atmospheric turbulence and the telescope. In [4], the FT of the random medium is modeled as a stationary random process with independent zero-mean Gaussian real and imaginary parts. It is shown that the average bispectrum of the transfer function $\hat{B}_p(w_1, w_2)$ is strictly positive for all frequencies up to the diffraction limit. Therefore

$$\hat{B}_i(w_1, w_2) = B_o(w_1, w_2)\hat{B}_p(w_1, w_2),$$
$$\angle\hat{B}_i(w_1, w_2) = \angle B_o(w_1, w_2). \quad (9)$$

The phase information of the bispectrum of the object is given by the phase of the average bispectrum of the observed intensities. Usually, $\hat{B}_p(w_1, w_2)$ is obtained from accurate measurements of a point source. As pointed out in [12], it is desirable to use only the phase information in the reconstruction. Therefore, as in the previous model, our purpose is to retrieve the object of interest from its true bispectrum phase.

III. Uniqueness of the Reconstruction from the Phase Functions

The restoration of each projection is based on the fact that we have exact knowledge of its Fourier phase or its Bispectrum phase. Once we have this information we need to ensure that we can uniquely reconstruct the desired signal. We first show that it is possible to recover the sequence $F_\theta(\xi)$ from the phase of $G_\theta(\xi)$. Analogously, $B_{f\theta}(\xi_1, \xi_2)$ will be determined from the phase of $B_{g\theta}(\xi_1, \xi_2)$. To show that a sequence is uniquely specified by the phase only of its Fourier transform, Hayes *et al.* [13] set the conditions under which this is possible:

Theorem 1: Let $x[n]$ and $y[n]$ be two finite sequences that are zero outside the interval $0 \le n \le N-1$ with Z-transforms that have no zeros in reciprocal pairs or on the unit circle.[1] If $\angle X(w) = \angle Y(w)$ at $N-1$ distinct frequencies in the interval $0 < w < \pi$, then $x[n] = \beta y[n]$ for some positive constant β.

A consequence of this theorem is the following:

Corollary 1: Let $x[n]$ be a finite sequence that is zero outside the interval $0 \le n \le N-1$ and where zeros are $N-1 = K-1+4P+2P^*$, where $(K-1)$ is the number of nonreciprocal zeros, and P and P^* are the number of reciprocal and real reciprocal pairs, respectively. There is a unique sequence $y[n]$, except for some positive constant factor, that is zero outside the interval $0 \le n \le K-1$ for which $\angle X(w) = \angle Y(w)$ at $N-1$ distinct frequencies in the interval $0 < w < \pi$.

We have created a new set of conditions to reconstruct a sequence from another with the same Fourier phase but different length. This is the case of projections blurred by a zero phase OTF. The reconstruction is only possible if the Z transform of $x[n]$ has the same zeros as the Z transform of $y[n]$ plus, necessarily, the rest of the zeros in reciprocal pairs. In our case, these zeros will correspond to the zeros of the PSF. The proof of Corollary 1 follows from considering that it is false and leading to a contradiction of Theorem 1. To identify the sequence $y[n]$, only $K-1$ points of its Fourier phase are needed. However, our original signal $x[n]$ is specified by $N-1$ points of its Fourier phase. Therefore, we need $N-1$ points to ensure that all information about $y[n]$ is contained in the Fourier phase of $x[n]$.

We are also interested in extending these results to 2-D sequences. This extension can be achieved by mapping the 2-D sequence into a 1-D sequence and then applying Theorem 1, although in this case, the election of the pairs of distinct frequencies (w_1, w_2) is not arbitrary (see Appendix A). Thus, it is possible to state a similar corollary for 2-D signals:

Corollary 2: If $x[n, m]$ is a finite sequence of dimensions $N \times N$, then there is a unique sequence $y[n, m]$, except for some positive constant factor, with dimensions $K \times K < N \times N$ such that $\angle X(w_1, w_2) = \angle Y(w_1, w_2)$ at $(N-1)^2$ distinct frequencies in the region $0 < w_1 < \pi, 0 < w_2 < \pi$.

Corollary 1 set the theoretical bases to reconstruct a 1-D signal degraded by a zero-phase OTF from the phase of the blurred signal. We can include the case of the linear-phase OTF only if it has been previously compensated. The first algorithm we develop in this correspondence is based on this result. Corollary 2 set the theoretical bases to reconstruct a 1-D signal degraded by a zero-phase or linear OTF from its bispectrum phase. This result motivates the second algorithm developed in this work.

[1] Although not demonstrated in [13], the theorem could be modified to allow zeros on the unit circle.

IV. Algorithms

In this section, we derive two different methodologies to solve the image restoration problem for the deterministic and random blur models. We assume that a sequence of images is provided. For example, we might have several observations of the same image embedded in noise with possibly different phase shifts, or a sequence of images of an object moving in a noisy background, or a sequence of short exposure speckle interferograms, etc.

The structure of both algorithms is motivated by the following facts:

1) To avoid the high complexity associated with the HOS of 2-D signals, we restore images from their projections.
2) Use of HOS allows reducing the presence of Gaussian noise while retaining phase information from the signal.
3) Reconstruction from the phase information can be motivated considering the following properties and common assumptions:
   a) The FT of a discrete finite length signal can be uniquely reconstructed from its phase (Corollary 1).
   b) Analogously, the bispectrum may be recovered from its phase (Corollary 2).
   c) The phase from many blurring functions is zero or linear.
4) Finally, the WS is chosen to retrieve the signal from its third-order moments since it is a robust and well-proven method.

Algorithm 1: The first algorithm is summarized in the following steps:

1) For each image of the sequence, compute the Radon transform to obtain the projections.

For each angle, do the following:

2) Estimate the bispectrum from the set of projections available.
3) Reconstruct the projections by means of the WS algorithm [9] (noise has been removed; however, the signal is still blurred).
4) From the Fourier phase, retrieve the desired signal.
5) Obtain the image applying the inverse Radon transform.

In the first step of the algorithm, the Radon transform is calculated from an interpolation of the Cartesian sampling grid to the polar grid of the 2-D FFT of the image. There is an intrinsic loss of information in this operation. However, using FFT lengths larger than the size of the image and using polynomial interpolations in each direction of order $(m-1)$ for $m \ge 2$ [15], we get good estimations for the projections. See [16] and references therein for other implementations of the Radon transform. In Step 2), we calculate the third moment sequence or the triple correlation in the frequency domain for each

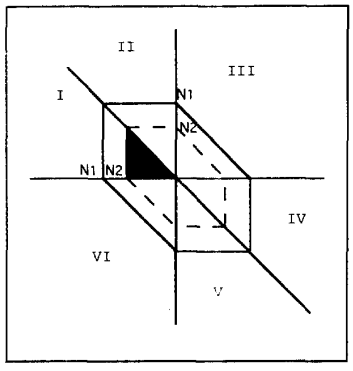

Fig. 1. Third-order moment region of support for sequences of length N_1 and N_2. The symmetry regions from I to VI are also shown.

projection and then average over the realizations of the projections at the same angle [6]. In Step 3), we obtain the estimated sequence through the WS algorithm, we only make use of the third-order moment sequence. In the next step, we obtain $f_\theta(s)$ from the phase of $g_\theta(s)$. We use an iterative algorithm similar to the one proposed in [13]. Some modifications are necessary to adapt the scheme to the new set of conditions. The algorithm is as follows:

1) Obtain the M-point DFT of $g_\theta(n)$ and derive its phase function $\varphi_{g\theta}(k) \quad k = 0, \cdots, M-1$, where $M \geq 2N$.
2) Form another sequence $y_{i\theta}(n)$ given by

$$y_{i\theta}(n) = \begin{cases} 0 & 0 \leq n < Int(K/2) \\ f_{i\theta}(n) & Int(K/2) \leq n < [N - Int(K/2)] \\ 0 & [N - Int(K/2)] \leq n \leq M-1 \end{cases} \tag{10}$$

where $f_{1\theta}(n) = g_\theta(n)$, K is the length of the blurring filter, and $Int(x)$ indicates the closest integer smaller than x.
3) Obtain a new estimation $F_{i+1\theta}(k) = |Y_{i\theta}(k)| \exp[\varphi_{G\theta}(k)]$, where $Y_{i\theta}(k)$ is the M-point DFT of $y_{i\theta}(n)$, and $F_{i+1\theta}(k)$ is the M-point DFT of the new estimated signal $f_{i\theta}(n)$.

In the first iteration of Step 2, we use the blurred signal. We set to zero the left and right margins to obtain a signal with the same length than the one we are trying to reconstruct. That provides a convenient initial guess for the magnitude of the Fourier transform and at the same time speeds up the process.

Steps 2 and 3 are repeated until the algorithm converges. Finally, the inverse Radon transform is implemented reversing the Radon transform procedure.

It must be pointed out that any linear phase factor should be corrected before applying Step 4); otherwise, the iterative procedure will not converge to the right solution.

Algorithm 2: The second algorithm consists of the following steps:

1) For each image of the sequence, compute the Radon transform to obtain the projections.

For each angle, do the following:

2) Estimate the bispectrum from the set of projections available.
3) Retrieve the bispectrum of each original projection from its 2-D estimated phase.
4) Reconstruct the projections by means of the WS algorithm [9].
5) Obtain the reconstructed image applying the inverse Radon transform.

Steps 3) and 4) differ from the ones of the first algorithm. To retrieve the bispectrum of the original signal from the 2-D bispectrum

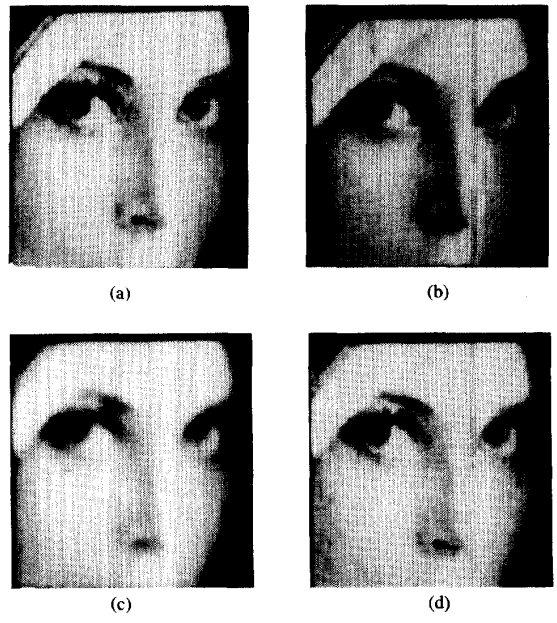

Fig. 2. (a) Original image; (b) image obtained after applying Radon and inverse Radon transform; (c) blurred image by a 5×5 Gaussian filter, $\alpha = 0.35$; (d) restored image from (c) using Algorithm 1.

phase of the blurred signal, we implement an analogous iterative algorithm to the one for 1-D sequences. The new intervals in Step 2 take into account the third-order moment region of support depicted in Fig. 1. For signals of length N_1, the third-order moment sequence is zero outside an outer hexagonal region [14]. Suppose we know the dimensions of the object to be N_2, where $N_2 < N_1$; in this case, the region of support is the inner hexagonal region. Its boundaries establish the new intervals in the iterative algorithm. We could also speed up the process by taking advantage of the symmetry regions of third-order moments and use only the samples in the region $0 \leq n_1 \leq N_1, 0 \leq n_2 \leq N_2, n_1 \geq n_2$. In Step 4) the WS Algorithm reconstructs the signal from its moments. After this step, any linear phase factor should be corrected before projecting back the image.

The computational burden of the two algorithms to restore each projection is given by

1) the sample estimation of the bispectrum, which is the same for both algorithms and of order $O(2KN^2)$, where K is the number of available realizations and N the length of the signal
2) the WS, which requires $O(20/3N^3)$ operations
3) the iterative reconstruction step, which differs for both algorithms.

Thus, Step 4) in Algorithm 1 entails a computational cost to $O(2I_1M_1 \log_2 M_1)$, where I_1 is the number of iterations, and M_1 is the size of the FFT. For Algorithm 2, Step 3) requires $O(2I_2M_2^2 \log_2 M_2^2)$ operations, where $M_2 \times M_2$ is the size of the 2D FFT.

V. Simulation Examples

Example 1: In this example, we examine the behavior of Algorithm 1 when an image is degraded by a zero-phase blurring filter. Fig. 2(a) shows a 64×64 image, and Fig. 2(b) shows the same image after applying the Radon transform followed by the inverse Radon transform, where the 2-D FFT's to compute the projections are 256×128. Fig. 2(c) is a blurred version of this image with

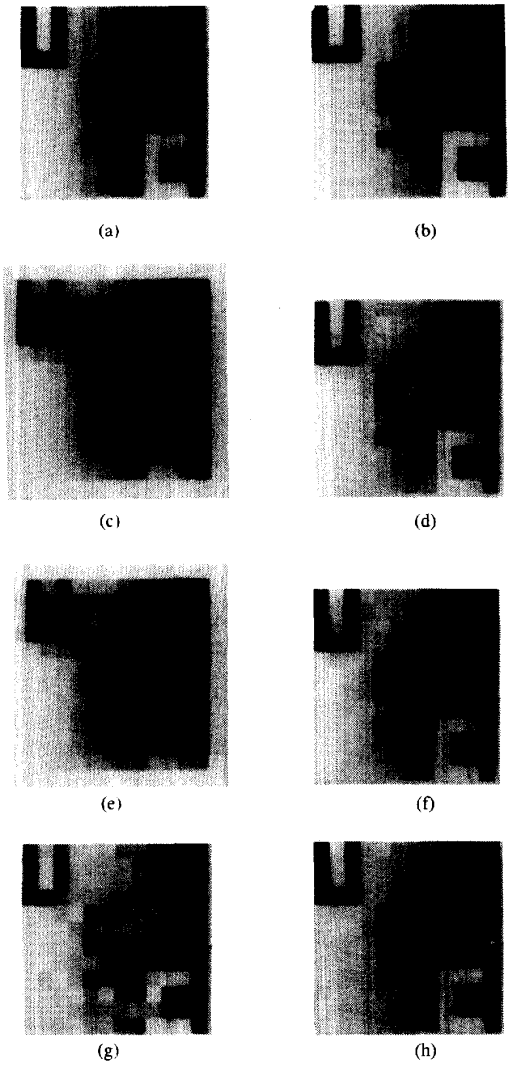

Fig. 3. (a) Original image; (b) image obtained after applying Radon and inverse Radon transform; (c) blurred image by a 3×3 Gaussian filter $\alpha = 0.7$; (d) restored image from (c) using Algorithm 1; (e) same as (c) but SNR = 25 dB; (f) restored image from (e) using Algorithm 1; (g) restored image using parametric Wiener filter; (h) restored image using parametric Wiener filter and the true phase of the signal.

a 5×5 Gaussian filter, with $\alpha = 0.35$. Fig. 2(d) is the restored image from the Fourier phase using Algorithm 1. Steps 2) and 3) are not performed since no noise is present. From this image, we see that high frequencies have been properly recovered. However, we observe some distortion. This is due to a slight relative shift among projections.

Example 2: In this example, we show the performance of the first algorithm and compare the restoration when other existing methods are applied. The original image is a computer-generated image shown in Fig. 3(a). The reconstructed image after applying the Radon transform followed by the inverse Radon transform is shown in Fig. 3(b). Fig. 3(c) presents a blurred version of this image when a 3×3 Gaussian filter with $\alpha = 0.7$ is utilized. Fig. 3(d) shows the restored image obtained from Algorithm 1. The phase reconstruction step is applied with FFT's of dimension 128 and 50 iterations. In

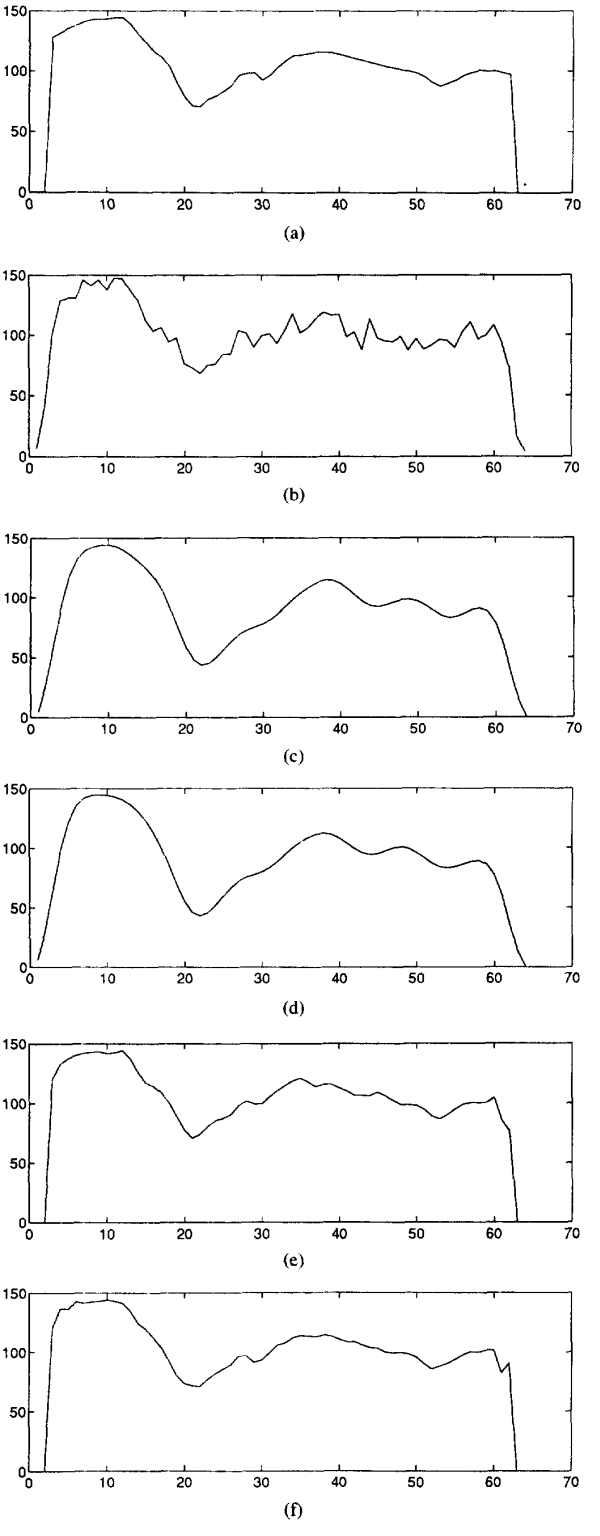

Fig. 4. (a) Original projection at angle 0°; (b) degraded projection, blurred by a 5×5 Gaussian filter, $\alpha = 0.9$, SNR = 5 dB; (c) restored signal using parametric Wiener filter; (d) restored signal using the magnitude of the Wiener filter and the true phase of the signal; (e) restored signal using Algorithm 1; (f) restored signal using Algorithm 2.

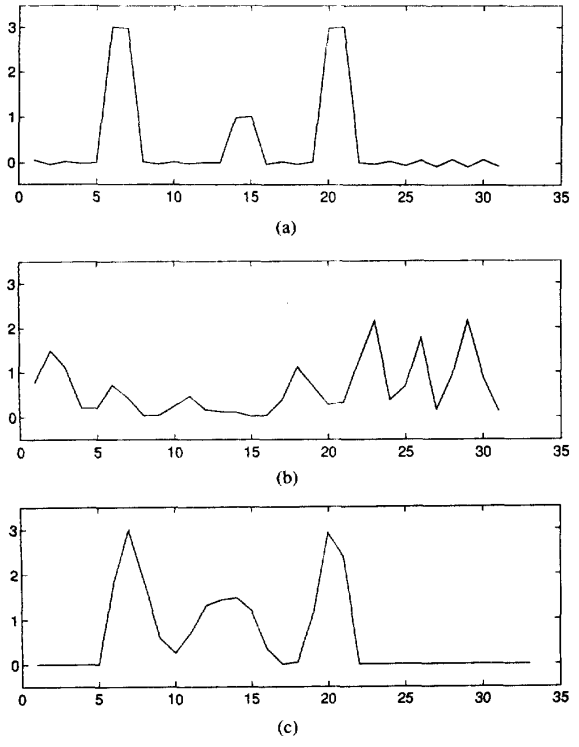

Fig. 5. (a) Projection of a diffracted image of three stars; (b) one of the 300 simulated speckle interferograms; (c) solution from the reconstructed bispectrum using Algorithm 2 and assuming length 16.

Fig. 3(e), the image is blurred with the same filter, and Gaussian noise for SNR = 25 dB is added. The restored image is shown in Fig. 3(f) when Algorithm 1 is used. The third-order moments are estimated from 50 shifted realizations. To compare this result with a correlation-based method, we consider in Fig. 3(g) the parametric Wiener filter, where the periodogram-based estimates of the power spectra of the noise and the image are obtained considering 50 noisy realizations [17]. A modified version of this filter is suggested in [18], where the Fourier phase of the restored image is estimated from the bispectrum. In Fig. 3(h), we show the restored image from the magnitude of the parametric Wiener filter and the true phase of the signal. As we can observe, the method proposed in this correspondence gives better results than the Wiener filter and similar results when the true phase is incorporated. However, we must point out that the proposed restoration scheme does not make use of the blurring filter: only its size. In this sense, this method realizes a blind restoration.

Example 3: In this experiment, we compare the algorithms in a low SNR scenario. Fig. 4(a) corresponds to the projection of the image in Fig. 2(a) at angle 0°. Fig. 4(b) corresponds to the same projection when the image is degraded by a 5×5 Gaussian blurring filter with $\alpha = 0.9$ and the SNR = 5 dB. Fifty noisy and randomly shifted realizations are available. The results using the parametric Wiener filter and the modified Wiener filter are shown in Fig. 4(c) and (d). The small details have been lost, and even if we use the true phase of the signal, we cannot properly restore the original projection. Fig. 4(e) and (f) show the results using Algorithm 1 and Algorithm 2, respectively, where the FFT size and the number of iterations are 256 and 50 for the first algorithm and 256×256 and 25 for the second one. The restoration is better accomplished by Algorithm 2 (except at the extreme of the signal) at the expense of a higher computational cost. We clearly see that high frequencies are better preserved, and the error is much lower when the proposed algorithms are utilized. Unfortunately, for this low SNR, although the quality of the 1-D projection has been considerably improved, small error contributions from all projections will propagate and add up to the final image. In order to avoid this effect, we should apply HOS-based methods directly to the image.

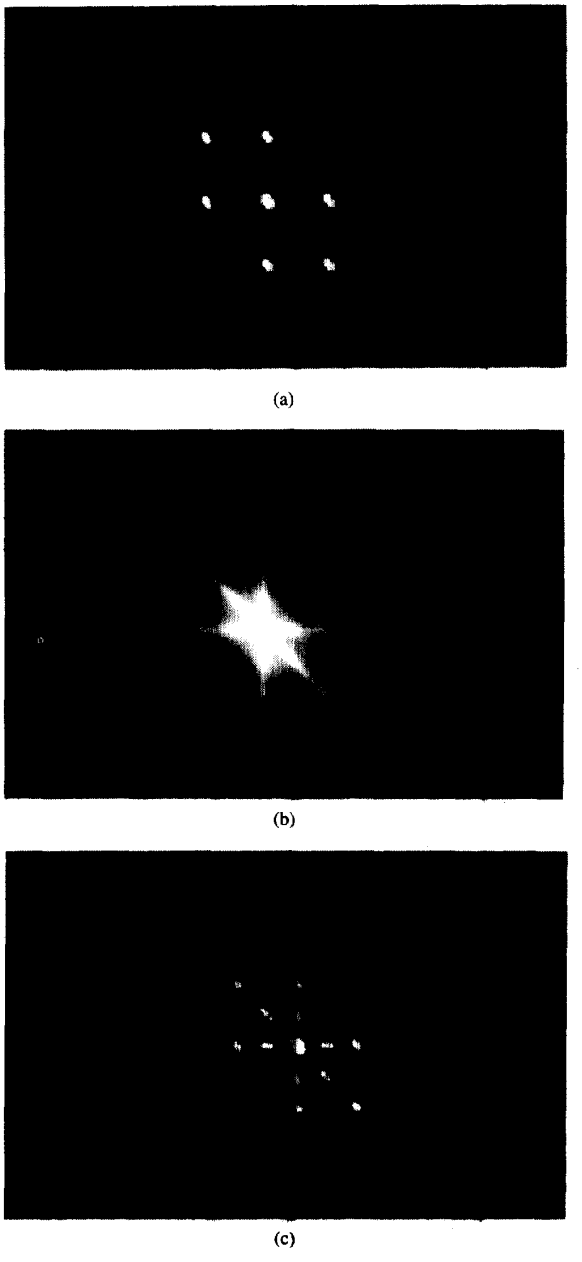

Fig. 6. (a) Third-order moment for the projection of Fig. 5(a); (b) average third-order moment interferogram; (c) reconstructed third-order moment from the iterative step in Algorithm 2.

Example 4: We have simulated a sequence of short exposure speckle interferograms assuming Gaussian statistics for the atmos-

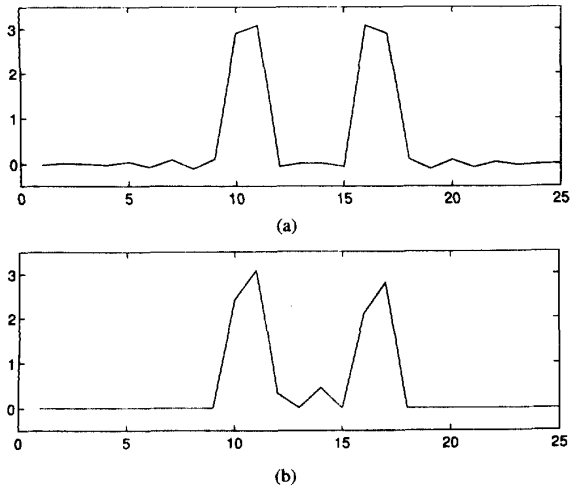

Fig. 7. (a) Projection of a diffracted image of two stars; (b) solution from the reconstructed bispectrum using Algorithm 2 and assuming length 8.

phere. Assuming that we know the dimensions of the object, we uniquely reconstruct the third-order moment sequence from the phase of $\hat{B}_i(w_1, w_2)$ by means of Algorithm 2. Fig. 5(a) shows a projection of a group of three simulated stars of different intensities. The image was diffracted through a rectangular pupil function. Fig. 5(b) shows one of the 300 interferograms that were generated using Gaussian distribution for the real and imaginary part of the FT of the random medium. The reconstructed signal using Algorithm 2 is depicted in Fig. 5(c), where we assumed that the length of the three stars was 16 samples. Fig. 6(a) shows the third-order moment of the original projection, whereas Fig. 6(b) shows the average third-order moments computed from the interferograms. In Fig. 6(c), the third-order moment sequence of the object has been estimated through Step 3) of Algorithm 2 using 2-D FFT's of sizes 256×256 with 150 iterations. Fig. 7(a) shows a projection of a group of two simulated stars. Fig. 7(b) shows the reconstructed signal using Algorithm 2 from 300 speckle interferograms assuming a length equal to eight samples. Fig. 8(a) shows the image of the two simulated stars. Fig. 8(b) is one of the 300 speckle interferograms. Finally, Fig. 8(c) shows the reconstructed image.

Example 5: In this example, we apply Algorithm 2 to real astronomical images. They were provided by the Astrophysics Institute of Canaries and recorded from the "William Herschel" 4.2–m telescope at the Observatory of Roque de los Muchachos. Fig. 9 is one of the 300 speckle interferograms of size 256×256 that corresponds to a binary star separated 0.4 s-arc (ADS 4265). Fig. 10(a) shows one of the projections at 0° (vertical projection). Several choices for the length at this angle were given and found that the two stars were visible for length around 20 pixels. Algorithm 2 was employed using 2-D FFT's of sizes 512×512 with 25 iterations. The estimated projection is shown in Fig. 10(b).

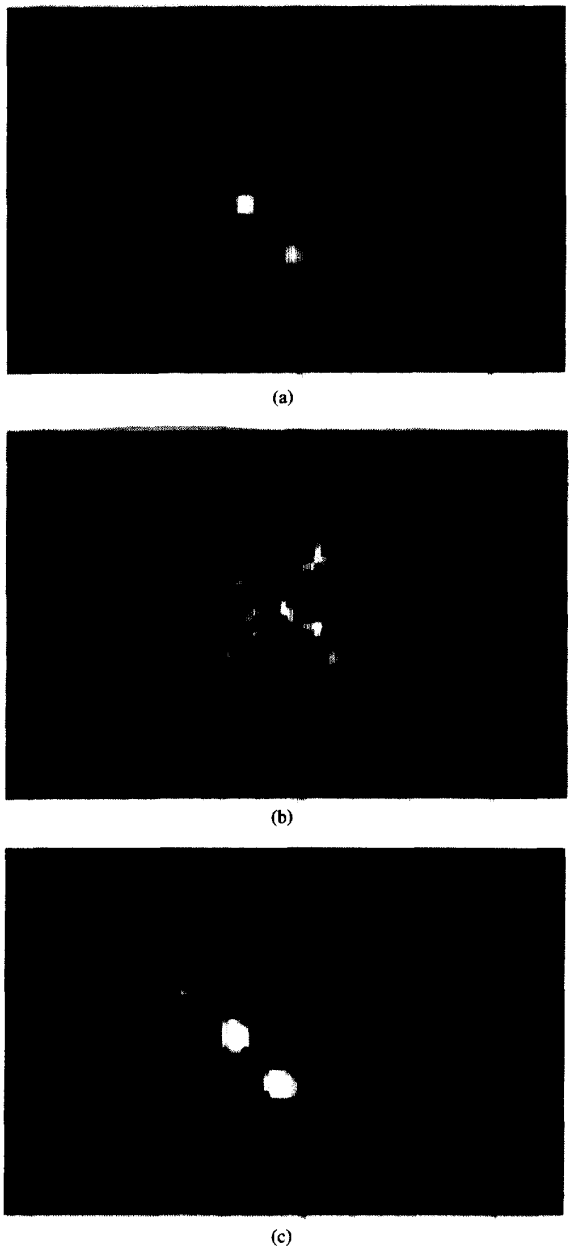

Fig. 8. (a) Simulated double star; (b) one of the 300 speckle interferograms using Gaussian statistics for the atmosphere; (c) restored image using Algorithm 2.

VI. Conclusions

In this correspondence, we have shown that it is possible to restore degraded images from the HOS of its projections. Two different approaches were given to reconstruct the 1-D signals from either the phase of the Fourier transform or the phase of the bispectrum. They were applied to images distorted with deterministic PSF and Gaussian noise and to simulated astronomical images degraded by turbulent atmosphere of known statistics. The motivation behind the use of these methods is the following. First, using HOS allows us to reduce the effects of the noise and at the same time obtain an estimate of the Fourier phase or the bispectrum phase of the signal that leads to the original signal. Second, employing the projections of the image reduces the high complexity associate with HOS of images. The capability of the WS to reconstruct the projections from its third-order moments is demonstrated. Furthermore, for the case of deterministic PSF, the blurring filter was not used: only its size. Although the complexity using HOS over 2-D signals is reduced, the computational load is still high. Nevertheless, the quality of the

Fig. 9. One of the 300 speckle interferograms of size 256 × 256 that corresponds to a binary star

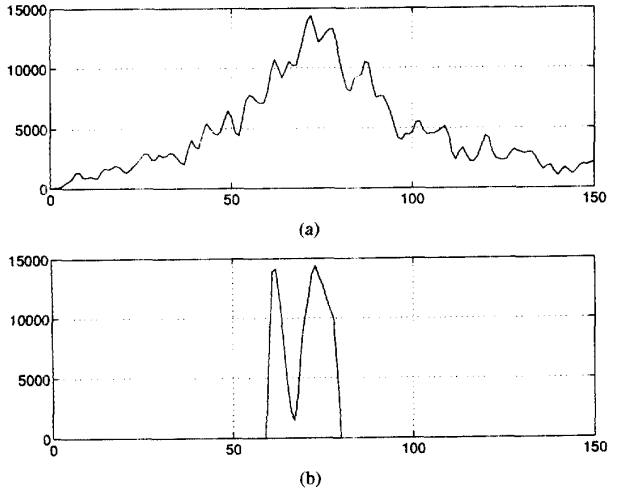

Fig. 10. One of the projections at 0° (vertical projection); (b) estimated projection.

images shown in this work was considerably improved. The results proved to be quite good for moderate SNR. For low SNR, the restoration of the projections was also good, although small errors in some of the projections are easily propagated to the image. It is necessary to avoid using projections for strongly degraded images. However, the analytical complexity grows considerably when the bispectrum of an image (not the projections), which is a 4-D signal, is estimated. Future work should be directed toward low-cost procedures to extract the phase information from the bispectra of images as well as low-cost HOS-based restoration methods.

APPENDIX A

The 2-D discrete Fourier transform of an $N \times N$ 2-D signal $f(n_1, n_2)$ is defined as

$$F(w_1, w_2) = \sum_{n_1=0}^{N-1} \sum_{n_2=0}^{N-1} f(n_1, n_2) e^{-jw_1 n_1} e^{-jw_2 n_2}.$$

Denoting by

$$x(w_1, n_2) = \sum_{n_1=0}^{N-1} f(n_1, n_2) e^{-jw_1 n_1}$$

then

$$F(w_1, w_2) = \sum_{n_2=0}^{N-1} x(w_1, n_2) e^{-jw_2 n_2}.$$

$F(w_1, w_2)$, and $x(w_1, n_2)$ can be seen as a 1-D Fourier pair with parameter w_1. Therefore, applying Theorem 1, we can obtain $x(w_1, n_2)$ from the phase of $F(w_1, w_2)$ at any $N-1$ distinct w_2 frequencies. Analogously, we can see $x(w_1, n_2)$ and $f(n_1, n_2)$ as a 1-D Fourier pair with parameter n_2 and thus recover $f(n_1, n_2)$ from the phase of $x(w_1, n_2)$ at any $N-1$ distinct w_1 frequencies. Hence, $(N-1)(N-1)$ points of the phase of $F(w_1, w_2)$ in $0 < w_1 < \pi$, $0 < w_2 < \pi$ are needed to reconstruct $f(w_1, n_2)$. Since w_1 has been used as a fixed parameter in the first place, the pairs (w_1, w_2) are not arbitrarily taken. Although w_1 could be placed at any $N-1$ distinct frequencies, they must remain the same for any w_2. Thus, the grid of frequencies (w_1, w_2) forms $N-1$ aligned columns in w_1 of $N-1$ points arbitrarily distributed in w_2.

REFERENCES

[1] S. A. Dianat and M. R. Raghuveer, "Fast algorithms for phase and magnitude reconstruction from bispectra," *Opt. Eng.*, vol. 29, no. 5, pp. 504–512, May 1990.

[2] B. M. Sadler, "Shift and rotation invariant object reconstruction using bispectrum," in *Proc. Workshop HOS Anal.*, Vail, CO, June 1989, pp. 106–111.

[3] V. Chandran and S. Elgar, "Position, rotation, and scale invariant recognition of images using higher-order spectra," in *Proc. ICASSP 92*, San Francisco, pp. 213–216.

[4] A. W. Lohmann, G. Weigelt, and B. Wirnitzer, "Speckle masking in astronomy: Triple correlation theory and applications," *Applied Opt.*, vol. 22, no. 24, pp. 4028–4037, Dec. 1983.

[5] A. W. Lohmann and B. Wirnitzer, "Triple correlations," *Proc. IEEE*, vol. 72, no. 7, pp. 889–901, July 1984.

[6] C. L. Nikias and A. P. Petropulu, *Higher-Order Spectra Analysis: A Nonlinear Signal Processing Framework.* Englewood Cliffs, NJ: Prentice-Hall, 1993.

[7] E. Sayrol, C. L. Nikias, and T. Gasull, "Image restoration using higher-order statistics and the radon transform," in *Proc. IEEE Signal Processing Workshop HOS*, South Lake Tahoe, CA , June 1993, pp. 76–80.

[8] A. P. Petropulu and C. L. Nikias, "Signal reconstruction from the phase of the bispectrum," *IEEE Trans. Signal Processing*, vol. 40, no. 3, pp. 601–610, Mar. 1992.

[9] J. A. Fonollosa and J. Vidal, "System identification using a linear combination of cumulant slices," *IEEE Trans. Signal Processing*, vol. 41, no. 7, pp. 2405–2412, July 1993.

[10] S. R. Deans, *The Radon Transform and Some of Its Applications.* New York: Wiley-Interscience, 1983.

[11] M. I. Sezan, G. Pavlovic, and M. Tekalp, "On modeling the focus blur on Image restoration," in *Proc. ICASSP 92*, Albuquerque, NM, pp. 2485–2488.

[12] J. C. Dainty, "Bispectrum imaging through turbulence," in *Proc. Workshop HOS Anal.*, Vail, CO, June 1989, pp. 130–133.

[13] M. H. Hayes, J. S. Lim, and A. V. Oppenheim, "Signal reconstruction from the phase or magnitude," *IEEE Trans. Acoust., Speech, Signal Processing*, vol. 28, no. 6, pp. 672–680, Dec. 1980.

[14] J. M. Mendel, "Tutorial on higher-order statistics (spectra) in signal processing and system theory: Theoretical results and some applications," *Proc. IEEE*, vol. 79, no. 3, pp. 278–305, Nov. 1991.

[15] W. H. Press, B. P. Flannery, S. A. Teulovsky, and W. T. Vetterling, *Numerical Recipes in C.* Cambridge, UK: Cambridge University Press, 1990.

[16] M. Tabei and M. Ueda, "Backprojection by upsampled Fourier series expansion and interpolated FFT," *IEEE Trans. Image Processing*, vol. 1, no. 1, pp. 77–87, Jan. 1992.

[17] H. C. Andrews and B. R. Hunt, *Digital Image Restoration.* Englewood Cliffs, NJ: Prentice-Hall, 1979, p. 144.

[18] M. G. Kang, K. T. Lay, and A. K. Katsaggelos, "Phase estimation using the bispectrum and its application to image restoration," *Opt. Eng.*, vol. 30, no. 7, pp. 976–985, July 1991.

[19] J. Goodman, *Statistical Optics.* New York: Wiley-Interscience, 1985, pp. 402–450.